minerals

MDPI

Article

Sequential Transformation Behavior of Iron-Bearing Minerals during Underground Coal Gasification

Shuqin Liu *, Weiping Ma, Yixin Zhang, Yanjun Zhang and Kaili Qi

School of Chemical and Environmental Engineering, China University of Mining and Technology (Beijing), Beijing 100083, China; 13260239766@163.com (W.M.); zhangyixin_1123@163.com (Y.Z.); MRZYJUN@163.com (Y.Z.); kelly5263@163.com (K.Q.)

* Correspondence: liushuqin@cumtb.edu.cn; Tel.: +86-10-6233-9156

Received: 31 December 2017; Accepted: 12 February 2018; Published: 28 February 2018

Abstract: Detailed mineralogical information from underground coal gasification (UCG) is essential to better understand the chemical reactions far below the surface. It is of great scientific significance to study the mineral transformation and identify the typical minerals in certain process conditions, because it may help to ensure the stable operation of gasification processes and improve the utilization efficiency of coal seams. The transformation of iron-bearing minerals has the typical characteristics during the UCG process and is expected to indicate the process parameters. In this paper, UCG progress was subdivided into pyrolysis, reduction and oxidation stages, and the progressive coal conversion products were prepared. Two types of lignite with different iron contents, Ulankarma and Ulanqab coals, were used in this study. The minerals in the coal transformation products were identified by X-ray diffraction (XRD) and a scanning electron microscope coupled with an energy-dispersive spectrometer (SEM-EDS). The thermodynamic calculation performed using the phase diagram of FactSage 7.1 was used to help to understand the transformation of minerals. The results indicate that the transformation behavior of iron-bearing minerals in the two lignites are similar during the pyrolysis process, in which pyrite (FeS_2) in the raw coal is gradually converted into pyrrhotite ($Fe_{1-x}S$). In the reduction stage, pyrrhotite is transformed into magnetite (Fe_3O_4) and then changes to FeO. The reaction of FeO and Al_2O_3 in the low iron coal produces hercynite above 1000 °C because of the difference in the contents of Si and Al, while in the high iron coal, FeO reacts with SiO_2 to generate augite ($Fe_2Si_2O_6$). When the temperature increases to 1400 °C, both hercynite and augite are converted to the thermodynamically-stable sekaninaite.

Keywords: underground coal gasification; hyper-iron coal; coal ash; mineralogy

1. Introduction

During high-temperature coal combustion and gasification at high temperatures, the reactivity differences of organic matters in coal can be almost ignored, while the transformation behavior of minerals becomes important to the stability of the process [1]. The reactions of inorganic minerals during combustion and gasification include a series of complicated physical and chemical changes that eventually form ash and slag with complex compositions [2]. Hence, detailed information about the mineralogical properties of coal ash is not only essential to optimize the operation parameters during coal utilization, but also significant for improving coal utilization efficiency and identifying the impacts of solid wastes on the environment.

Underground coal gasification (UCG) is the process of in situ conversion of coal directly into combustible gaseous products. A sketch of the UCG process is shown in Figure 1 [1]. The first step of UCG is to choose a proper location and then design and construct an underground reactor [3]. Boreholes are drilled from the surface to the coal seam, followed by a horizontal channel connecting the boreholes along the bottom of the coal bed. After a gasifier is prepared, the coal at one end of the

channel is ignited, and gasification agents such as air, oxygen and steam are injected into the reactor. Accompanied by a series of coal reactions including pyrolysis, reduction and oxidation, the combustible gas is discharged from the production borehole [4]. UCG is carried out in the underground coal bed without physical coal mining, transportation or coal preparation, which is regarded as supplementary to the coal mining method. The composition and heat value of the product gas depends on the initial gas injected, the position for gas injection and the temperature profile of the coal bed.

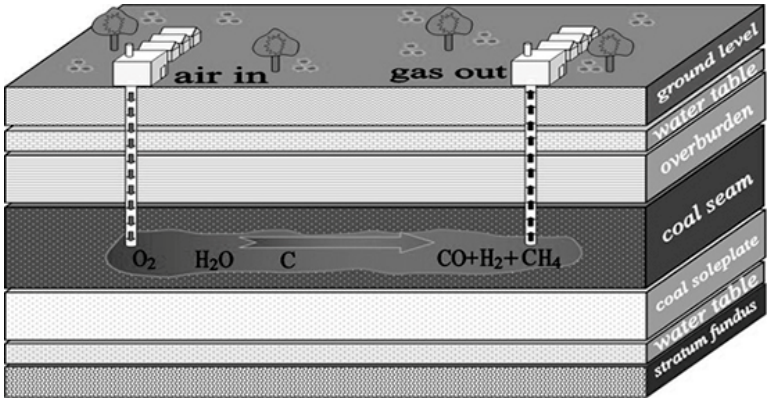

Figure 1. Sketch of the underground coal gasification (UCG) process.

Because UCG is always performed within the coal seam, several hundred meters beneath the surface, only the injection and production parameters (temperature, pressure, flow) can be determined. It is particularly difficult to determine the actual reaction conditions, especially the temperature field distribution and thermal equilibrium of the underground gasifier. Therefore, it is necessary to investigate the relationship between gasification technology and mineralogical characteristics of ash and slag through UCG simulation experiments [5]. On the other hand, the potential for groundwater pollution from UCG-generated residue has also been a concern in recent years [6]. The leaching behavior of toxic elements from solid residues is closely related to the characteristics of UCG ash and slag.

Numerous research papers have been published on the conversion of minerals during coal combustion, but only a few papers have reported on the transformation of minerals during coal gasification [7,8]. Most of the study of ash chemistry during the high-temperature gasification process has focused on the investigation of ash deposition and slag formation and on the difficulties found in industrial gasifiers regarding fluidized bed gasification and entrained flow gasification [9,10]. However, few papers focus on the formation mechanism of ash and slag during the UCG process [11].

Mineral transformation occurs at elevated temperatures, including chemical reactions between the clay minerals, carbonate minerals, pyrite and quartz in the coal [12–14]. The reaction rate and degree were greatly affected by temperature. Generally, the softening temperature of minerals in the gasification condition was found to be lower than that in the combustion condition [15]. The fusible minerals, such as the carbonate, sulfate minerals and feldspar, tend to become a "solvent mineral" at high temperatures, which promotes the melting and slagging of gasification residues [16]. In addition to temperature, the furnace type is another important factor for ash formation behaviors [17].

There are few reports on the formation and properties of UCG slag [18]. In the USA, a series of residues and rocks was sampled from the UCG test site near Centralia, Washington. X-ray diffraction (XRD) and a scanning electron microscope coupled to an electron microprobe (SEM-EDS) were used to analyze the mineralogical characteristics of the samples, and a moderate temperature reaction was confirmed [19]. Reduced iron reacted with clay minerals to form a solid solution of aluminum-rich hercynite ($FeAl_2O_4$), which then serves as the precursor and reacts with SiO_2 at high temperatures to form sekaninaite ($Fe_2Al_4Si_5O_{18}$) [20–23].

Iron-bearing minerals have been the focus of many studies [24]. The iron element can reduce the melting point of ash and will largely control the ash slagging property. Fe^{2+} also reduces the viscosity of the aluminosilicate melt and accelerates the sintering process of the ash deposits. During the combustion process, the iron-bearing mineral is particularly easy to react with sulfur to form ash and sediment [25–27]. In this study, based on the first UCG field test of lignite, laboratory UCG simulation tests were performed to prepare UCG semi-coke (800 °C) and ash in different atmospheres. XRD and SEM-EDS were used to identify the composition and microstructure of the typical minerals formed and existing in UCG ash and slag, which help to understand the transformation of iron-bearing minerals during the UCG process [28].

2. Experiment and Modeling

2.1. Coal Sampling and Analysis

Ulanqab and Ulankarma lignites are used in this study. The Ulanqab lignite is from a neighboring coal mine of the UCG field test area, which is located in Gonggou coal field, Ulanqab, Inner Mongolia, China. The coal bed has an average depth of 280 m. The Ulankarma lignite is taken from Shengli coal field, Inner Mongolia, China. The coal samples are collected according to the collection standard and then are crushed, ground and sieved before analysis.

Proximate analysis and ultimate analysis were carried out based on ASTM Standards D3173-11 (2011) [29], D3175-11 (2011) [30] and D3174-11 (2011) [31]. The total sulfur content was analyzed following ASTM Standard D3177-02 (2002) [32]. A scanning wave-length dispersive X-ray fluorescence spectrometer (XRF; Thermo ARL Advant'XP+, Xenemetrix, Round Rock, TX, USA) was used to determine the major-element oxides (SiO_2, TiO_2, Al_2O_3, Fe_2O_3, MgO, CaO, MnO, Na_2O, K_2O and P_2O_5) in high-temperature ashes (815 °C) of the samples, which were prepared as pressed powder mounts. The loss on ignition (LOI) for each sample was also determined at this temperature.

2.2. Experimental Installation

The multifunctional pyrolysis/gasification experimental system (HWD-500, Beijing Henven Scientific Instrument Factory, Beijing, China) is used to determine the reaction extent and residence time for coal pyrolysis, semi-coke reduction and residual-coke oxidation during the UCG process. We use the apparatus to complete independent pyrolysis and gasification experiments, accomplish temperature control, agent control and mass metrology. The highest work temperature is up to 1300 °C; the range of heating rate is 0.1–20 °C/min; and the mass measurement is 500 g. The schematic diagram is shown in Figure 2. CO_2 and N_2 are supplied by a high-pressure gas cylinder whose pressure and flow are controlled using a needle valve; the air is supplied by the air compressor; the plunger pump automatically inhales distilled water and then pumps the steam generator to produce steam. The pressure gauge is used to indicate intake agent flow. N_2 is a protective gas, and CO_2/H_2O (g) is the gasification gas. The oxidizing agent enters into thermobalance and reacts with coal/char to form pyrolysis gas/coal gas. Thereafter, the gas is purified by a cold water bath and secondary tar absorption device and then dried by the dryer; finally, flow is measured through a wet-type gas flowmeter. The sampling port is used to collect the gas to measure the gas composition at different times.

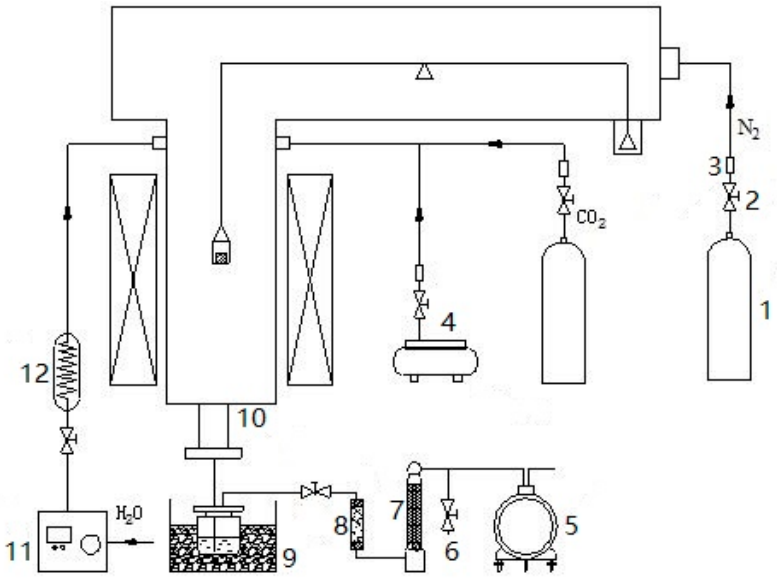

Figure 2. Multifunctional pyrolysis/gasification experimental system. 1, Cylinders; 2, needle valve; 3, pressure gauge; 4, air compressor; 5, wet-type gas flowmeter; 6, sampling port; 7, dryer; 8, secondary tar absorption device; 9, cold water bath; 10, thermobalance; 11, plunger pump; 12, steam generator.

Char/slag preparation in different reaction conditions is conducted using a high-temperature pipe furnace (SK-G08163, Tianjin Zhonghuan Furnace Corp., Tianjin, China), which is a batch-type high-temperature tubular resistance furnace. The heating element is a silicon-molybdenum bar; the furnace adopts a TY/PMF ceramic fiber sheet; and the furnace tube is corundum material. The working temperature in the furnace is up to 1600 °C, and temperature control is programmed with an accuracy of ±1 °C. The range of pressure is −0.10~0.05 MPa. A schematic of the high-temperature tube furnace is shown in Figure 3. CO_2 and N_2 are supplied by a high-pressure gas cylinder, whose pressure and flow are controlled by a needle valve; the air is supplied by an air compressor; H_2O (g) is produced by a steam generator. N_2, CO_2/H_2O (g), and air enter into thermobalance and then react with coal/char to form pyrolysis gas/coal gas. Thereafter, the gas is purified by a tar absorption device and a wash bottle. After the furnace reaches room temperature, char/slag is taken out for analysis.

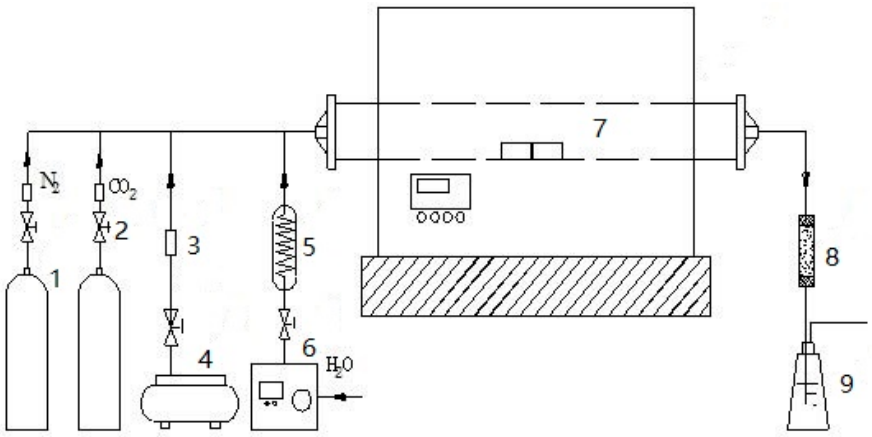

Figure 3. High-temperature tube furnace. 1, Cylinders; 2, needle valve; 3, pressure gauge; 4, air compressor; 5, water steam generator; 6, plunger pump; 7, high temperature tube furnace; 8, tar absorber; 9, gas bottle.

2.3. Preparation of Sequential Transformation Products

2.3.1. Determination of Reaction Conditions

The purpose of this test is to confirm the reaction conditions for the preparation of semi-coke, ash under reduced atmosphere and ash under oxidized atmosphere. Specifically, the aim of the part is to clarify the reaction time and reaction extent of pyrolysis, reduction and the oxidation process.

According to the mechanism of UCG and practical reaction condition, assumptions were made as follows:

(1) Methane is derived from the coal pyrolysis process.
(2) The final gas consists of pyrolysis gas and gasification gas.
(3) The highest temperature of the pyrolysis reaction was set as 800 °C.
(4) The temperature of the oxidation zone was 200 °C higher than that of corresponding gasification zone.

Based on the above assumptions, the multifunctional pyrolysis/gasification experimental system was used for determining the reaction condition (mainly reaction time) of pyrolysis, reduction and the oxidation process.

(1) Coal samples were placed in a multifunctional pyrolysis/gasification experimental system with N_2 (2 L/min) protective atmosphere from room temperature to 800 °C at a heating rate of 5 °C/min and constant temperature for 30 min. The release of pyrolysis products finished, and the thermobalance did not continue to lose weight.
(2) With the reduction agent of H_2O (g) (5 g/min) and CO_2 (2 L/min), the completion times (t_2) of the reduction process from 900–1300 °C were 55 min, 40 min, 25 min, 15 min and 20 min, respectively. Among these, the completion time of the 1300 °C gasification process was 20 min, which was longer than that of the 1200 °C gasification process. The reason was that the melting degree of slag at 1300 °C was stronger than that at 1200 °C, and the melting slag partially coated unburned carbon and then hindered the reaction of the reduction agent with carbon.
(3) With the oxidation agent of air, the completion time (t_3) of the oxidation process from 1100–1500 °C was about 60 min. Due to the low oxygen concentration of air, the oxidation process at different temperatures had little difference. Thus, the reaction time of each oxidation final temperature (t_3) was 60 min.

2.3.2. Preparation of Semi-Coke/Ash/Slag

According to the atmosphere and flow rate in the conversion conditions, as well as the residence time corresponding to different final temperature conditions, we used the high-temperature tube furnace to prepare semi-coke (800 °C), ash under reduced atmosphere (900–1300 °C) and ash under oxidized atmosphere (1100–1500 °C). The product should be cooled to room temperature for analysis and characterization.

2.4. Sample Analysis

2.4.1. XRD Analysis

The ash samples were crushed, ground and sieved. Samples below 75 μm were selected for XRD analysis, which was performed on a powder diffractometer (D/max-2500/pc XRD, Rigaku, Japan) with Ni-filtered Cu-Kα radiation and a scintillation detector. The XRD pattern was recorded over a 2θ range of 2°–90° at a scan rate of 8°/min and a step size of 0.02°. Jade 5.0 (MDI, Livermore, CA, USA) software was used to analyze the XRD curve for qualitative analysis [33].

2.4.2. SEM-EDS Analysis

The raw coal and char and slag samples were firstly crushed, ground and sieved. The particles below 75 μm were collected for SEM-EDS analysis. A field emission scanning electron microscope (FE-SEM, MERLIN Compact, Zeiss, Jena, Germany) and an energy dispersive X-ray spectrometer (EDS, INCA, Oxford, UK) were used to study the morphology of the minerals and to determine the distribution of minerals [34]. The samples were prepared under low-vacuum SEM conditions. The analytical conditions were as follows: working distance 9.2~12.4 mm, beam voltage 15.0 kV. The images were captured via a secondary electron detector.

2.4.3. Thermodynamic Modeling

FactSage was introduced in 2001 as the fusion of two well-known software packages in the field of computational thermochemistry: F*A*C*T/FACT-Win and ChemSage. The thermochemistry models can be used to analyze equilibrium conditions for reactions occurring between inorganic and/or organic materials, as well as providing insight into the mineral formation speciation. The database can assist in understanding, as well as predicting what can and will happen with specific coal and mineral sources inside the gasification process [35]. In this study, thermodynamic equilibrium modeling was conducted using the "Equilib" and "Phase diagram" module in FactSage 7.1, which is the Gibbs energy minimization workhorse of FactSage. It calculates the concentrations of chemical species when specific elements or compounds reacting or partially reacting to reach a state of chemical equilibrium.

FactSage is used to calculate the phase diagram of Al_2O_3–SiO_2–FeO and Al_2O_3–SiO_2–Fe_2O_3 for analyzing the effect of ash composition on final mineral composition and transformation. For the calculations, the equilibrium module was employed together with the databases Ftoxid and FactPs. Additionally, the solution phases of Ftoxid-SLAG and Ftoxid-oPyr (databases) were selected to simulate the gasification. During the reduction stage, the temperature was changed from 900–1300 °C in 50 °C increments; the total pressure is 1 atm; and the partial pressure of (CO, H_2) is 0.1 atm. The iron oxide is input in the form of FeO. In the oxidation process, the temperature varies from 1100–1500 °C in 50 °C increments; the total pressure is 1 atm; and the partial pressure of O_2 is 0.21 atm. The iron oxide is input in the form of Fe_2O_3.

3. Results and Discussion

3.1. Coal Analysis

The results of the ultimate and proximate analyses of the coal samples are shown in Table 1. It is shown that the ash yield in Ulankarma lignite is only 7.81%, while in Ulanqab lignite, it is 36.62%. Ulankarma lignite has more than a 3% sulfur content, which belongs to hyper-sulfur coal, while at the Ulanqab lignite, it is less than 0.5%.

Table 1. Proximate and ultimate analysis of coals (%).

Samples	Proximate Analysis/%				Ultimate Analysis/%				
	M_{ad}	A_{ad}	V_{ad}	FC_{ad}	C_{ad}	H_{ad}	O_{ad}	N_{ad}	$S_{t,ad}$
Ulanqab	9.22	32.62	34.00	33.38	45.22	3.16	8.70	0.64	0.44
Ulankarma	17.90	7.81	28.60	45.69	54.33	2.42	14.06	0.70	3.39

M, moisture; A, ash; V, volatile matter; FC, fixed carbon; C, carbon; H, hydrogen; O, oxygen; N, nitrogen; St, total sulfur; ad, air dry basis.

The percentages of major element oxides, as well as loss on ignition, for the Ulanqab and Ulankarma lignites are listed in Table 2.

Table 2. Percentages of major element oxides (%), and loss on ignition (LOI, %), and base to acid ratio (B/A).

Samples	SiO_2	Al_2O_3	Fe_2O_3	CaO	TiO_2	MgO	K_2O	Na_2O	MnO_2	SO_3	P_2O_5	LOI	B/A
Ulanqab	61.55	16.58	5.10	5.59	0.75	2.68	2.50	0.85	0.07	2.46	0.11	1.72	0.22
Ulankarma	30.91	8.98	38.43	6.58	0.53	1.57	0.53	0.50	0.04	6.75	0.05	5.48	1.18

The two lignites have substantially different ash components. The content of Fe_2O_3 in Ulankarma lignite is very high, as shown in Table 2, which is a typical hyper-iron coal [36] and has high sulfur content in this case. The total of SiO_2 and Al_2O_3 content in Ulanqab lignite is about 80%, while that in Ulankarma lignite is less than 40%. In the Ulankarma lignite, low content of SiO_2 and Al_2O_3, as well as high content of Fe_2O_3 and CaO result in lower ash melting points. The analysis results of the coal ash fusibility in a weakly-reducing atmosphere are exhibited in Table 3 [37]. It can be seen from Table 3 that the softening temperature of Ulankarma lignite ash is 1060 °C, but it is 1210 °C for Ulanqab lignite ash. In general, iron could reduce the melting point of coal ash.

Table 3. Coal ash fusibility (°C) in a weakly-reducing atmosphere.

Ash Melting Point	Ulanqab	Ulankarma
Deformation Temperature (DT)	1160	1060
Softening Temperature (ST)	1210	1060
Hemispherical Temperature (HT)	1230	1070
Fluid Temperature (FT)	1260	1080

3.2. Mineral Composition in Raw Coals

X-ray diffraction analysis was used to identify the typical minerals and mineral transformation behavior that occurs during the UCG process. The XRD analysis showed that the major minerals found in the Ulanqab lignite consist of quartz (SiO_2), muscovite ($KAl_2Si_3AlO_{10}(OH)_2$) and orthoclase ($KAlSi_3O_8$). Quartz is the most common mineral in coal [38,39]. Clay minerals are the most important components in coal, and in many cases, they are intimately associated with organic matter in coal [40,41]. The main minerals in Ulanqab lignite are in good agreement with the content of SiO_2 and Al_2O_3 in the ash.

The main minerals found in the Ulankarma lignite are quartz, kaolinite ($Al_2Si_2O_5(OH)_4$), gypsum ($CaSO_4 \cdot 2H_2O$) and pyrite (FeS_2). Kaolinite is also the main component of the clay mineral. Gypsum and pyrite are consistent with the high content of CaO and Fe_2O_3, respectively, in the Ulankarma lignite. High contents of gypsum and pyrite have also been observed in the lignites in the adjacent coal deposit, Shengli, in Inner Mongolia [42,43].

3.3. Minerals Transformation during Coal Pyrolysis

As shown in Figure 4a, the main minerals in 800 °C pyrolysis of semi-coke consist of quartz, muscovite and sanidine. It could be found from the comparison of the mineral composition between raw coal and semi-coke that orthoclase was present in raw coal, but not present in semi-coke, while sanidine is formed. Although the quartz and muscovite do not change, the characteristic peaks of quartz and muscovite in the pyrolysis semi-coke are significantly enhanced, indicating that there are increased contents of quartz and muscovite [44]. The decomposition of large amounts of volatile organic compounds during the pyrolysis process leads to the increases of the relative content of inorganic minerals. Furthermore, part of the aluminosilicate minerals are decomposed into SiO_2 under pyrolysis. Orthoclase and sanidine are feldspar minerals in the K-feldspar subfamily of homogeneous multiple variants. With the increase of temperature, the order of crystal structure of orthoclase is destroyed, and it is gradually transformed into completely disordered sanidine. The formation of sanidine at such a high temperature is consistent with its formation in coal and coal-bearing sequences.

For example, sanidine is a high-temperature mineral in altered volcanic ashes (tonsteins) and usually used as an indication of volcanic ash [45,46].

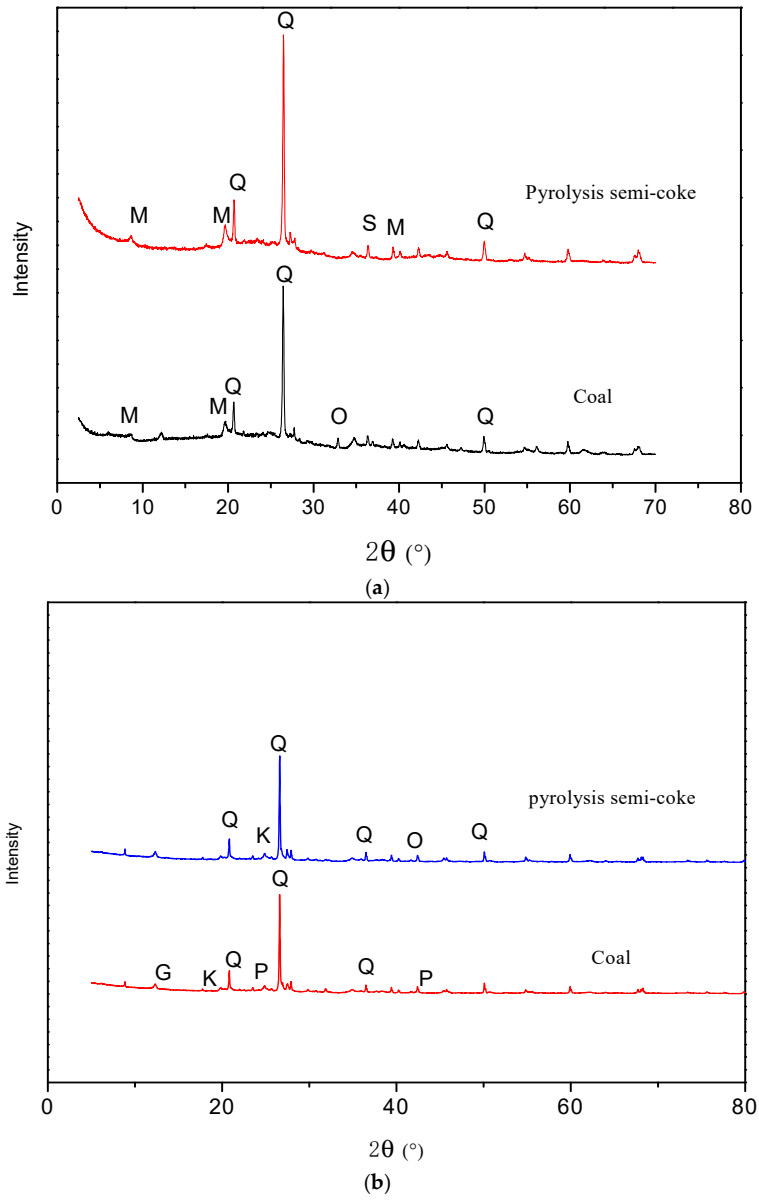

Figure 4. XRD patterns of coal and semi-coke (800 °C). (**a**) Ulanqab lignite; (**b**) Ulankarma lignite. Q—quartz; M—muscovite; S—sanidine; O—orthoclase; K—kaolinite; G—gypsum; P—pyrite.

As shown in Figure 4b, the main minerals in the semi-coke of Ulankarma lignite (800 °C) consist of quartz, kaolinite and orthoclase. Kaolinite starts to lose crystal water and is converted to metakaolinite above 327 °C [9], and then, the metakaolinite will decompose into γ-Al_2O_3 and SiO_2 around 827 °C [47]. The decomposition products of kaolinite can react with K_2O to produce orthoclase in the temperature range of 500–800 °C [48]. Therefore, it can be concluded that kaolinite is gradually decomposed during the pyrolysis process and is partially converted to orthoclase, but a small amount of kaolinite could still be found in the semi-coke because the pyrolysis temperature is relatively low.

As shown in the SEM image in Figure 5a, the material attached to the carbon particles is pyrite, which is consistent with the XRD results. After 800 °C pyrolysis, carbon content in the semi-coke rises because of the emission of the volatile organic matters. Fe and S elements are found on the carbon

particles in the semi-coke (Figure 5b), which is apparently present as pyrrhotite ($Fe_{1-x}S$) (x = 0–0.233) based on the analysis of the atomic ratio. The atomic ratio of Fe element to S element is 0.73:1 in Ulankarma semi-coke, which lies in the range of 0–0.233 [36]. This suggests that FeS_2 (in the coal) is gradually decomposed when the pyrolysis temperature is higher than 500 °C and S escapes in the form of S_2 (g). When the pyrolysis temperature reaches 800 °C, S escapes at a higher rate, and pyrrhotite is eventually formed with a molecular formula of $Fe_{0.73}S$ [8].

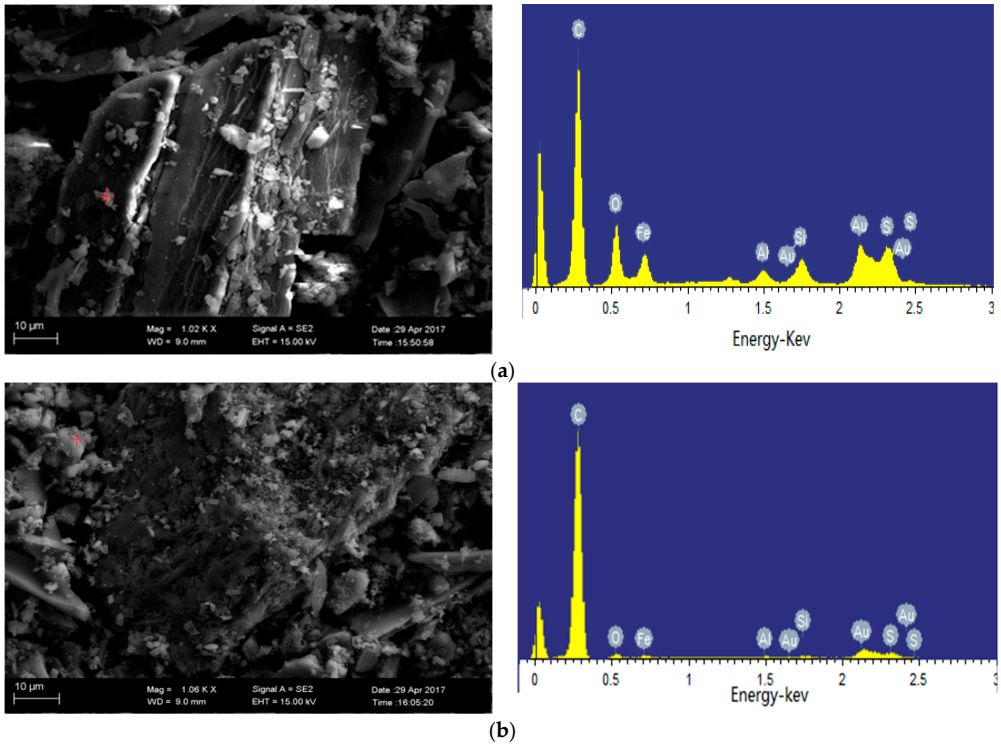

Figure 5. Iron-bearing minerals in Ulankarma lignite and its semi-coke (SEM-EDS secondary electron images). (**a**) Pyrite; (**b**) pyrrhotite.

3.4. Mineral Transformation during the Semi-Coke Reduction Process

Based on the results of XRD analysis in Figure 6a, the iron-containing mineral is present in the form of magnetite (Fe_3O_4) in the 900 °C reduction ash, which is converted from pyrrhotite. Sanidine is also present in the ash, but muscovite is not present in the pyrolysis semi-coke. The reason for the absence of the muscovite in the semi-coke is the gradual removal of the hydroxyl group under the action of high temperature. As the temperature rises above 900 °C, the demineralized muscovite reacts with CaO or FeO to produce orthoclase by the following reactions.

$$KAl_3Si_3O_{10} + CaO \rightarrow KalSi_3O_8 + CaO{\cdot}Al_2O_3$$

$$Kal_3Si_3O_{10} + FeO \rightarrow KalSi_3O_8 + FeO{\cdot}Al_2O_3$$

Magnetite is altered, while hercynite is formed in great quantities in the reduction ash at 1000 °C. It can be concluded that the magnetite in the reduction ash of Ulanqab is gradually transformed to FeO at a higher temperature and stronger reducing atmosphere. Then, FeO reacts with Al_2O_3 to produce hercynite at the 1000 °C gasification conditions. When the temperature reaches 1100 °C, the diffraction peak intensity of hercynite is further enhanced, which indicates that its content increases with temperature. Thereafter, at 1200 °C, the diffraction peak intensity of the hercynite declines, indicating that the content begins to decrease. Until 1300 °C, hercynite minerals decrease in abundance and are accompanied by the emergence of sekaninaite. As the thermodynamic properties of sekaninaite

are more stable, hercynite is converted to sekaninaite above 1300 °C. The result is completely in accordance with the report by McCarthy et al. (1988) [19], which proposes the medium temperature reaction in the study of slag from the UCG field test.

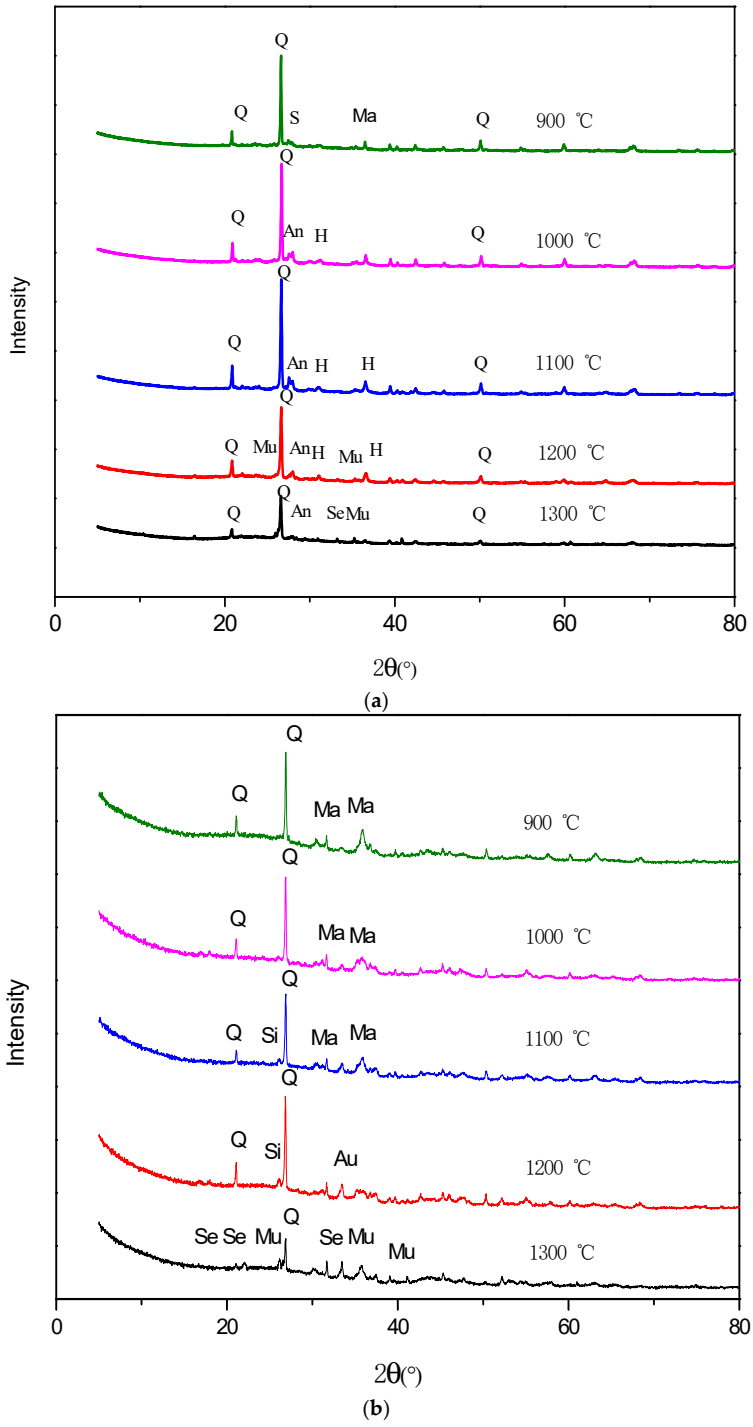

Figure 6. XRD patterns of the ash under reduced atmosphere (900–1300 °C). (**a**) Ulanqab lignite; (**b**) Ulankarma lignite. Q—quartz; Se—sekaninaite; Ma—magnetite; H—hercynite; An—anorthite; Mu—mullite; S—sanidine. Si—sillimanite; Au—augite; Se—sekaninaite.

Anorthite ($CaAl_2Si_2O_8$) is present in the reduction ash of Ulanqab lignite. Anorthite has also been detected in some volcanic ash influenced coals [49] and is an indication of a high-temperature mineral.

Anorthite is detected at 1000 °C and formed in great quantities at 1100 °C, and then, its content gradually decreases at 1200 °C. With the appearance of anorthite and the increase in content, quartz continues to decrease. Therefore, it can be concluded that quartz is involved as a reactant in the formation of anorthite. It is also inferred that Al_2O_3 and SiO_2 from the decomposition of orthoclase and anorthoclase react with CaO from the decomposition of augite to form anorthite, and the specific reaction is as follows [8,20,37,42].

$$CaO + Al_2O_3 + 2SiO_2 \rightarrow CaAl_2Si_2O_8$$

As shown in the XRD image in Figure 6b. Magnetite is found in the reduction ash of Ulankarma at 900 °C, which is in agreement with Ulanqab lignite, and the magnetite is also present in the temperature range of 1000–1100 °C.

Magnetite is present at the same time as augite ($Fe_2Si_2O_6$) in the reduction ash at 1200 °C. The reaction process is similar to that of the hercynite, and the magnetite is reduced to FeO at a higher temperature, then it reacts with the decomposition products of the orthoclase and kaolinite. Hercynite is present in the reduction ash of Ulanqab in the temperature range of 1000–1200 °C [50]. While hercynite is not present in the reduction ash of Ulankarma at 1200 °C, augite is formed in great quantities. A possible reason for this phenomenon could be explained as follows: The hercynite is not conducive to forming due to the low content of Al_2O_3 in the ash of Ulankarma. The SiO_2 content is relatively high, and the augite is conditionally formed. Augite is transformed to sekaninaite, the thermodynamically-stable mineral, at a high temperature of 1300 °C.

The orthoclase and kaolinite in the semi-coke are completely decomposed at a high temperature of 900 °C. Sillimanite has formed at 1100 °C and is produced in large quantities at 1200 °C. After 1300 °C, the sillimanite is no longer present, but mullite has started to form. The Al_2O_3 and SiO_2, which are respectively decomposition products of orthoclase and kaolinite in the semi-coke, n to produce sillimanite. As the temperature increases, sillimanite is converted to mullite, n-stable mineral [51]. The reaction process is as follows:

$$Al_2O_3 + SiO_2 \rightarrow Al_2SiO_5$$

$$Al_2SiO_5 + 2Al_2O_3 + SiO_2 \rightarrow Al_6Si_2O_{13}$$

Compared to the Ulanqab lignite, anorthite is not present in the reduction ash of the Ulankarma lignite. This is because of the low content of Al_2O_3 in the Ulankarma ash, resulting in the absence of anorthite. The diffraction intensity of the mineral in the reduction ash at 1300 °C is weak, indicating that the crystal minerals have disappeared and the ash has been melted, which is very close to the ash melting point of the Ulankarma lignite.

In the XRD analysis, hercynite is proven to exist in the reduction ash of Ulanqab at 1000 °C, and a small amount of augite minerals is also found in the SEM (Figure 7a). Therefore, augite and hercynite coexist in the reduction ash at 1000 °C, but augite content is low. The content of Al_2O_3 and SiO_2 in the ash of Ulanqab lignite is high, but the FeO from the reduction of magnetite tends to react with Al_2O_3 to form hercynite. Only a small amount of FeO reacts with SiO_2 to generate augite. However, the Al_2O_3 in the Ulankarma ash is very low, and it is involved in the formation of the sillimanite and mullite, resulting in the Al_2O_3 that can react with FeO to almost disappear; thus, the reaction produces augite, rather than hercynite during the reduction process. Consistent with the results of XRD analysis, sekaninaite minerals as shown in Figure 7b are present in the ash reduction of Ulanqab lignite at 1300 °C.

As shown in the SEM image in Figure 8, the augite mineral phase appeared at 1200 °C in the Ulankarma reduction ash, and the sekaninaite phase is present at 1300 °C.

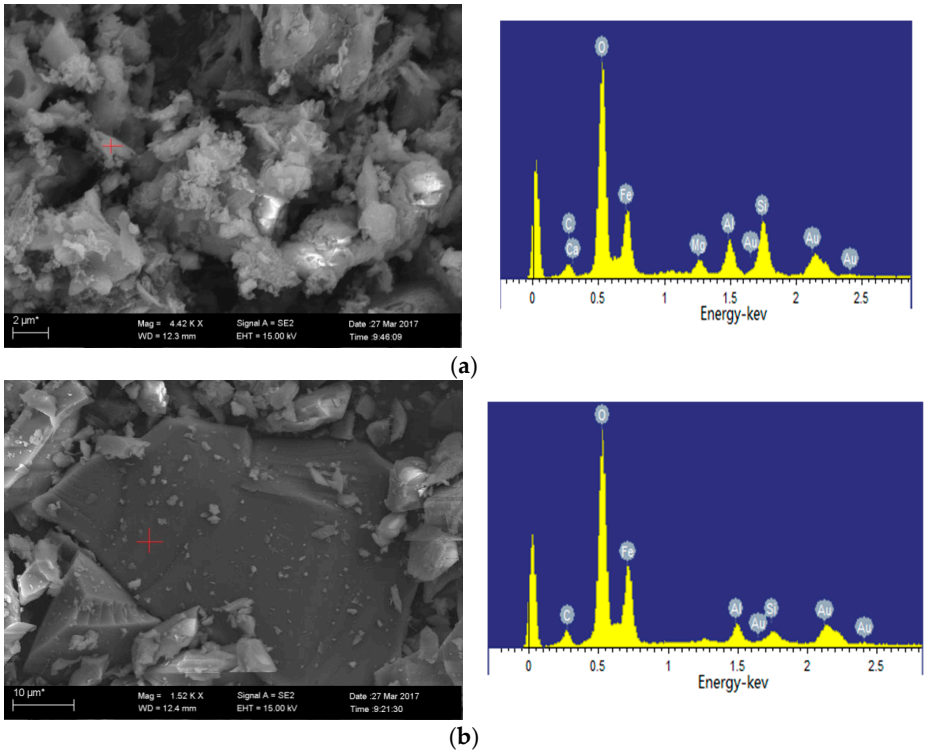

Figure 7. Minerals in reduction ash of Ulanqab lignite (SEM-EDS, secondary electron images). (**a**) Augite (1000 °C); (**b**) sekaninaite (1300 °C).

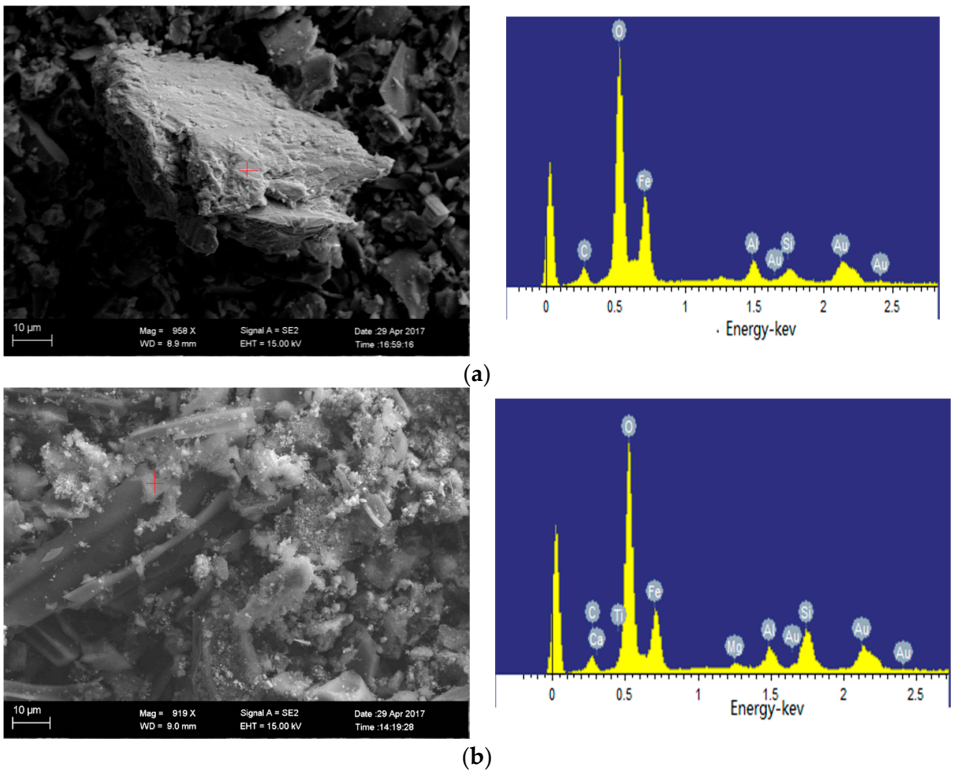

Figure 8. Minerals in reduction ash of Ulankarma lignite (SEM-EDS, secondary electron images). (**a**) Augite (1000 °C); (**b**) sekaninaite (1300 °C).

3.5. Mineral Transformation during Residual-Coke Oxidation Process

The XRD results of the oxidation ash of Ulanqab lignite are similar to the reduction ash in the mineral composition (Figure 9a). Hercynite and hematite are present in the 1100 °C oxidation ash at the same time. Hercynite decreases at 1200 °C, and then, trace amounts are observed at 1300 °C when massive hematite is formed in the oxidation ash. A possible reason for this change could be explained as follows: Fe^{2+} existing in hercynite reacts with the oxidizing agent, generating Fe^{3+} that is present in the form of hematite at 1100 °C, then the Fe^{2+} is continuously converted to hematite and finally completely transformed into hematite at 1300 °C. When the temperature reaches 1400 °C, the hematite is still present. Hematite is eventually transformed into thermodynamically-stable sekaninaite at high temperatures.

The content of hematite is reduced when the temperature reaches 1200 °C, although it should continue to rise theoretically with the transformation of hercynite. On the other hand, anorthite is generated at 1100 °C, but the anorthite content begins to decrease at 1200 °C. Finally, anorthite is absent at 1300 °C. Therefore, it is inferred that during the oxidation of Ulanqab lignite, low-temperature mixing occurs between the iron-bearing minerals and anorthite when the temperature reaches 1200 °C, which leads to the decrease of iron content and the absence of anorthite.

The content of quartz decreases at temperatures ranging from 1100–1300 °C, since it participates in the formation of minerals such as mullite and anorthite. When the temperature reaches 1400 °C, the quartz content is further reduced, while the cristobalite is formed in great quantities. This is because the quartz could change to form cristobalite at high temperatures [52]. The chemical properties of the cristobalite whose melting point is 1610 °C are extremely stable, so it is still present in the oxidation ash at 1500 °C.

The intensity of the XRD diffraction peak of the oxidation ash is weak at 1400 °C, indicating that the content of the crystal mineral is very low. Especially at 1500 °C, the crystal minerals in the ash are almost completely converted to the vitreous material, which is called vitrification. This phenomenon has also occurred in many ash-related studies. The vitrified ash is very stable, has no risk of leaching contamination and can be safely landfilled or used as a building material [53,54].

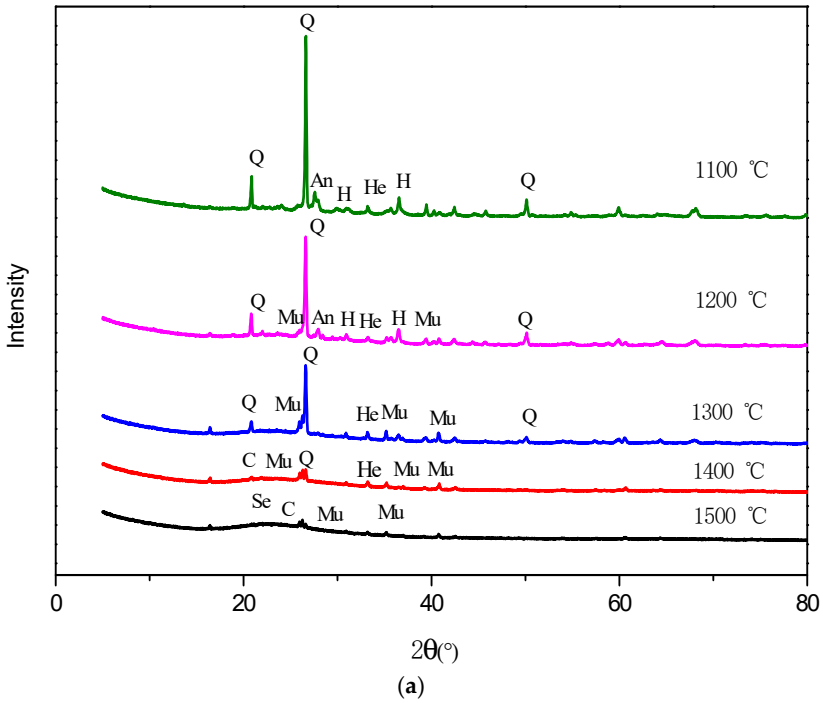

Figure 9. *Cont.*

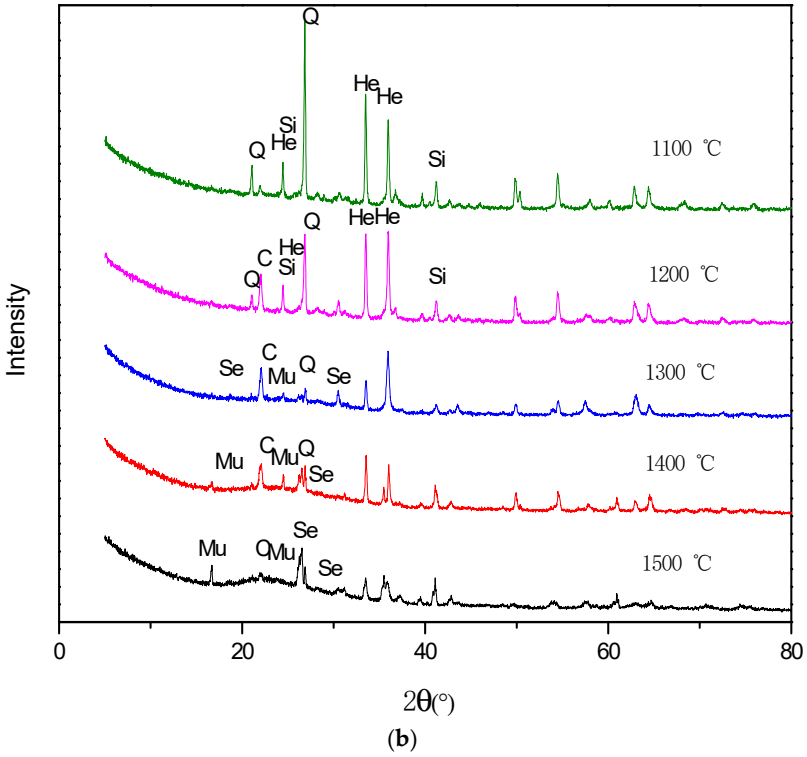

(**b**)

Figure 9. XRD patterns of the ash under oxidized atmosphere (1100–1500 °C). (**a**) Ulanqab lignite; (**b**) Ulankarma lignite. Q—quartz; An—anorthite; He—hematite; H—hercynite; Se—sekaninaite; C—cristobalite; Si—sillimanite; Mu—mullite.

The XRD results of the oxidation ash of Ulankarma lignite (Figure 9b) show that hematite could be found at the temperatures ranging from 1100–1200 °C. The magnetite is oxidized to hematite in an oxidizing atmosphere, and then, hematite is transformed to sekaninaite when the temperature is over 1300 °C. As the temperature reaches above 1400 °C, the content of the sekaninaite is still high. This is due to the high melting point of sekaninaite.

SEM images of 1100 °C ash and 1300 °C ash are shown in Figure 10a, b, respectively. The iron-bearing mineral is present in the form of hematite at 1100 °C oxidation ash, which is in agreement with the XRD analysis. The EDS analysis results of the mineral in Figure 10b show that the contained elements are complex, including Si, Al, Fe, Ca, K and Mg, and the content of each element is high. Thus, we can speculate that the mineral is ash. When the temperature reaches 1300 °C, the crystal minerals begin to melt largely due to the ash melting point of Ulankarma being 1060 °C.

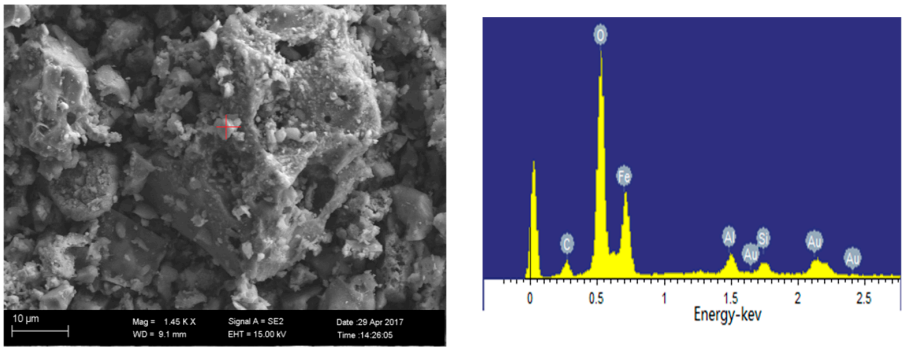

(**a**)

Figure 10. *Cont.*

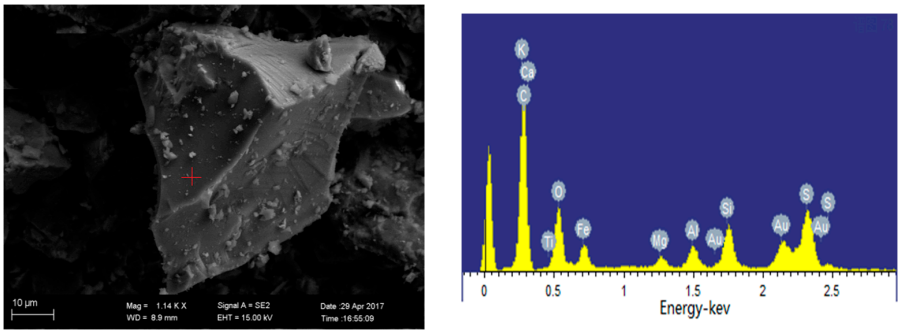

(**b**)

Figure 10. Minerals in oxidation ash of Ulankarma coal (SEM-EDS, secondary electron images). (**a**) 1100 °C; (**b**) 1300 °C.

As shown in the SEM image in Figure 11a, the hercynite appears in 1100 °C oxidation ash of Ulanqab lignite, which is consistent with the XRD analysis. Figure 11b shows that the low-temperature co-melt of iron-bearing minerals and calcium is formed when the temperature is below the ash melting point, which in turn leads to the decrease of crystal minerals in 1200 °C oxidation ash of Ulanqab lignite. Sekaninaite is stably present in 1400 °C since calcium is not present in oxidation ash of Ulankarma lignite.

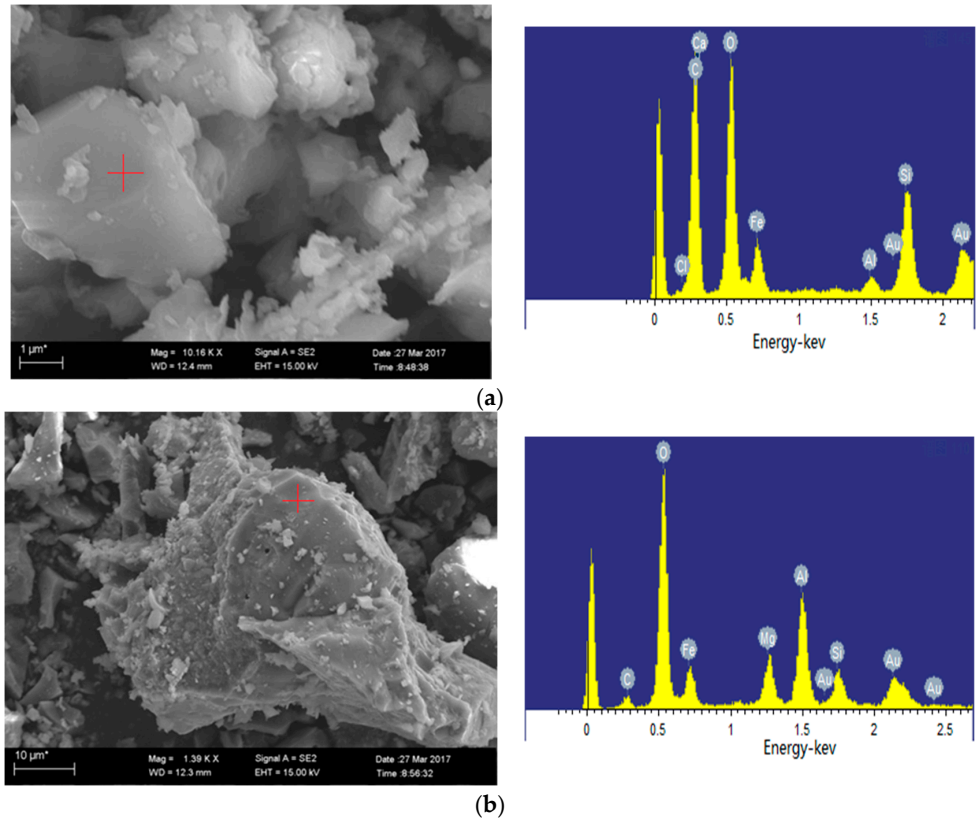

(**a**)

(**b**)

Figure 11. Minerals in oxidation ash of Ulanqab (SEM-EDS, secondary electron images). (**a**) Hercynite (1100 °C); (**b**) iron-bearing minerals and calcium feldspar co-melt at 1200 °C.

The sequential transformations of iron-bearing minerals with increasing temperature are displayed in Figure 12. Using XRD and SEM analyses, we can summarize that the composition of ash leads to the formation of typical iron-bearing minerals and affects the transformation of the

iron-bearing minerals. The transformation behavior of iron-bearing minerals in the two lignites is similar during the pyrolysis process, in which pyrite (FeS_2) in the raw coal is gradually desulfurized into pyrrhotite ($Fe_{1-x}S$). In the reduction stage, pyrrhotite is transformed into magnetite (Fe_3O_4) at 900 °C and then changes to FeO. Due to the difference in the content of Si and Al, the reaction of FeO and Al_2O_3 in the Ulanqab lignite produces hercynite above 1000 °C, while in the Ulankarma lignite, FeO reacts with SiO_2 to generate augite ($Fe_2Si_2O_6$). When the temperature rises to 1400 °C, both hercynite and augite are converted to the thermodynamically-stable mineral sekaninaite.

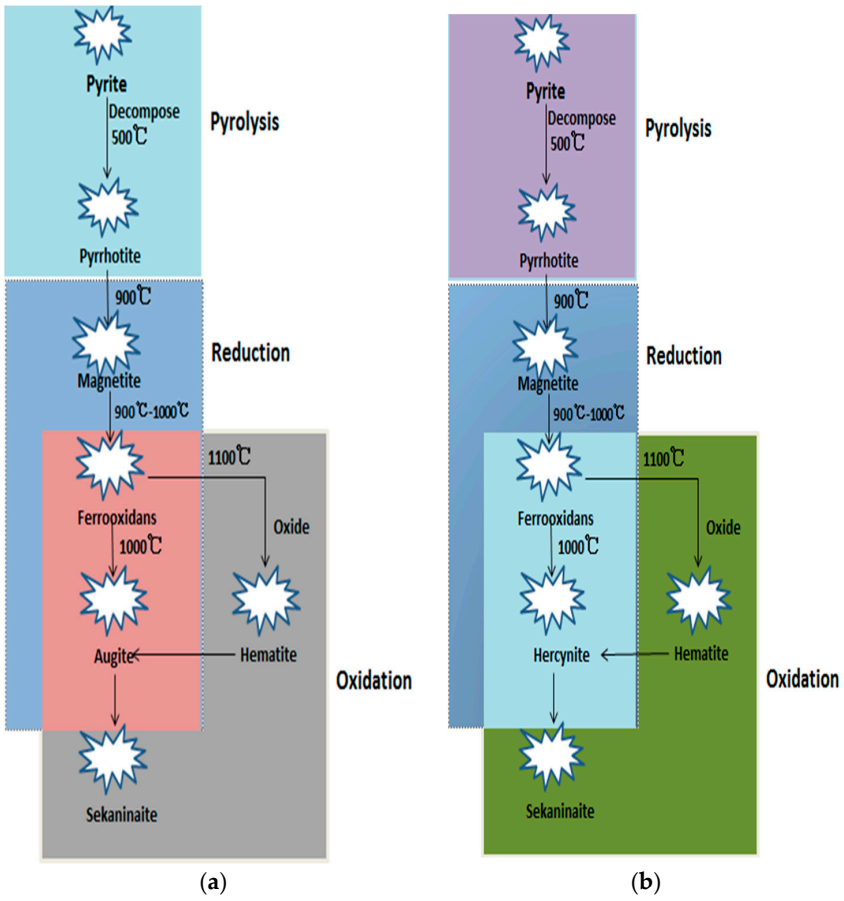

Figure 12. Sequential transformation of iron-bearing minerals in UCG process. (**a**) Ulankarma lignite; (**b**) Ulanqab lignite.

3.6. Thermodynamic Simulation of the Transformation of Iron-Bearing Minerals during Underground Coal Gasification

As shown in Figure 13, when the total of SiO_2 and Al_2O_3 content is about 0.8, it is easy to form aluminosilicate such as mullite. Quartz is formed in great quantities, while the cristobalite is less. The formation temperature of cristobalite is higher than 1400 °C. When the total of iron and aluminum content is about 0.7, hercynite is readily formed. Augite is observed when the total of iron and silicon content is above 0.6. As the temperature increases, both hercynite and augite are converted to sekaninaite, which is more thermodynamically stable. This is consistent with the previous experimental results.

As shown in Figure 14, mullite could be observed when the total of SiO_2 and Al_2O_3 content is about 0.6. The ash melting point is substantially higher when there is a high content of Si and Al. Quartz is formed in great quantities at temperatures ranging from 1350–1450 °C. Iron aluminate appears when the iron content is high, which is based on the content of Si and Al in raw coal.

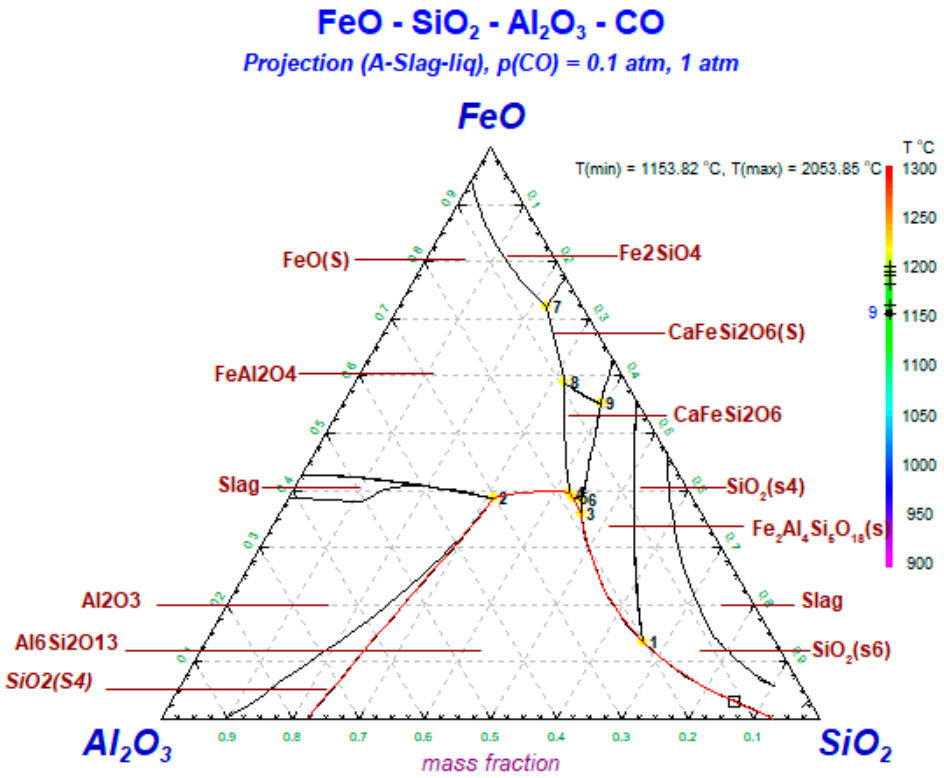

Figure 13. Phase diagram of Al_2O_3–SiO_2–FeO during reduction.

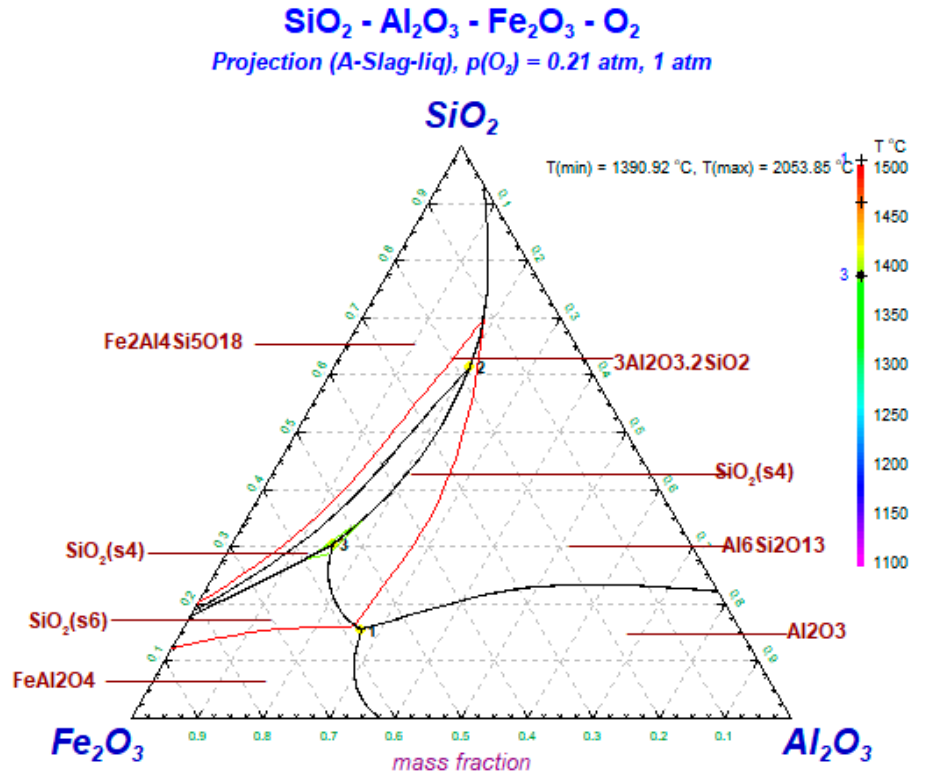

Figure 14. Phase diagram of Al_2O_3-SiO_2-Fe_2O_3 during oxidation.

4. Conclusions

(1) During the pyrolysis process, the iron-bearing minerals in the coal are transformed from pyrite (FeS_2) to pyrrhotite ($Fe_{1-x}S$).

(2) The typical iron-bearing minerals found in the ash under reduced atmosphere in the temperature range from 900–1300 °C involve magnetite (Fe_3O_4), ferrous oxide (FeO), hercynite ($FeAl_2O_4$) and augite ($FeSi_2O_6$). Magnetite changes to FeO, and then, FeO reacts with Al_2O_3 in the low-iron coal to produce hercynite at 1000 °C, while FeO reacts with SiO_2 in the hyper-iron coal to produce augite ($FeSi_2O_6$).

(3) The typical iron-bearing minerals during the oxidation process of residual-coke include hematite (Fe_2O_3), hercynite ($FeAl_2O_4$), augite ($FeSi_2O_6$) and sekaninaite ($Fe_2Al_4Si_5O_{18}$). Hematite in hyper-iron coal ash reacts with SiO_2 to produce augite, while in low-iron coal, it reacts with Al_2O_3 to form hercynite.

(4) Hercynite ($FeAl_2O_4$) and augite ($FeSi_2O_6$) are transformed into sekaninaite ($Fe_2Al_4Si_5O_{18}$) above 1400 °C.

Acknowledgments: The authors are grateful for the financial support provided by the Natural Science Foundation of China (No. 51476185). The authors wish to thank Shifeng Dai for his great support of the X-ray diffraction (XRD) and scanning electron microscope (SEM) analysis.

Author Contributions: Shuqin Liu conceived of, designed and performed the experiments and contributed reagents. Weiping Ma and Yixin Zhang performed the experiments, performed the X-ray diffraction (XRD) determination and thermodynamic simulation, observed the slag using SEM-EDS and analyzed the data. Yanjun Zhang and Kaili Qi analyzed the data. All authors participated in writing the manuscript.

Conflicts of Interest: The authors declare no conflict of interest.

References

1. Liu, S.; Qi, C.; Zhang, S.; Deng, Y. Minerals in the ash and slag from oxygen-enriched underground coal gasification. *Minerals* **2016**, *6*, 27. [CrossRef]
2. Li, W.; Bai, J. Mineral composition and characterization of coals and coal ashes. In *Chemistry of Ash from Coal*; Science Press: Beijing, China, 2013; pp. 1–7. (In Chinese)
3. Khadse, A.N.; Qayyumi, M.; Mahajani, S.M.; Aghalayam, P. Reactor model for the underground coal gasification (UCG) channel. *Int. J. Chem. React. Eng.* **2006**, *4*. [CrossRef]
4. Olateju, B.; Kumar, A. Techno-economic assessment of hydrogen production from underground coal gasification (UCG) in Western Canada with carbon capture and sequestration (CCS) for upgrading bitumen from oil sands. *Appl. Energy* **2013**, *111*, 428–440. [CrossRef]
5. Laciak, M.; Škvareková, E.; Durdan, M.; Kostur, K.; Wittenberger, G. Study of underground coal gasification (UCG) technology in laboratory conditions. *Chem. Listy* **2012**, *106*, 384–391.
6. Lutynski, M.; Suponik, T. Hydrocarbons removal from underground coal gasification water by organic adsorbents. *Physicochem. Probl. Miner. Process.* **2014**, *50*, 289–298.
7. Dai, S.; Seredin, V.V.; Ward, C.R.; Jiang, J.; Hower, J.C.; Song, X. Composition and modes of occurrence of minerals and elements in coal combustion products derived from high-Ge coals. *Int. J. Coal Geol.* **2014**, *121*, 79–97. [CrossRef]
8. Dai, S.; Zhao, L.; Peng, S.; Chou, C.L.; Wang, X.; Zhang, Y. Abundances and distribution of minerals and elements in high-alumina coal fly ash from the Jungar Power Plant, Inner Mongolia, China. *Int. J. Coal Geol.* **2010**, *81*, 320–332. [CrossRef]
9. Li, F.; Huang, J.; Fang, Y.; Wang, Y. Formation mechanism of slag during fluid-bed gasification of lignite. *Energy Fuels* **2011**, *25*, 273–280. [CrossRef]
10. Brooker, D. Chemistry of deposit formation in a coal gasification syngas cooler. *Fuel* **1993**, *72*, 665–670. [CrossRef]
11. Su, F.; Itakura, K.I.; Deguchi, G.; Ohga, K.; Kaiho, M. Evaluation of energy recovery from laboratory experiments and small-scale field tests of underground coal gasification (UCG). *Shigen-to-Sozai.* **2015**, *131*, 203–218. [CrossRef]

12. Reinmöller, M.; Klinger, M.; Schreiner, M.; Gutte, H. Relationship between ash fusion temperatures of ashes from hard coal, brown coal, and biomass and mineral phases under different atmospheres: A combined FactSage™ computational and network theoretical approach. *Fuel* **2015**, *151*, 118–123. [CrossRef]
13. McLennan, A.R.; Bryant, G.W.; Bailey, C.W.; Stanmore, B.R.; Wall, T.F. An experimental comparison of the ash formed from coals containing pyrite and siderite mineral in oxidizing and reducing conditions. *Energy Fuels* **2000**, *14*, 308–315. [CrossRef]
14. Wagner, N.J.; Coertzen, M.; Matjie, R.H.; Van Dyk, J.C. Coal gasification. In *Applied Coal Petrology*; Isabel, S.R., Crelling, J.C., Eds.; Elsevier: Amsterdam, The Netherlands, 2008; pp. 119–144.
15. Kapusta, K.; Wiatowski, M.; Stańczyk, K. An experimental ex-situ study of the suitability of a high moisture ortho-lignite for underground coal gasification (UCG) process. *Fuel* **2016**, *179*, 150–155. [CrossRef]
16. Matjie, R.H.; French, D.; Ward, C.R.; Pistorius, P.C.; Li, Z. Behaviour of coal mineral matter in sintering and slagging of ash during the gasification process. *Fuel Process. Technol.* **2011**, *92*, 1426–1433. [CrossRef]
17. Wu, X.; Zhang, Z.; Piao, G.; Xiang, H.; Chen, Y.; Kobayashi, N. Behavior of mineral matters in Chinese coal ash melting during char-CO_2/H_2O gasification reaction. *Energy Fuels* **2009**, *23*, 2420–2428. [CrossRef]
18. Chen, F.; Zhang, S.; Liu, G.; Pang, X. Method for Fracture Communication, Passage Processing, and Underground Gasification of Underground Carbon-Containing Organic Mineral Reservoir. U.S. Patent No. 14/430,446, 27 March 2014.
19. McCarthy, G.J.; Stevenso, R.J.; Oliver, R.L. Mineralogical characterization of the residues from the TONO I UCG experiment. In Proceedings of the Fourteenth Annual Underground Coal Gasification Symposium, Chicago, IL, USA, 15–18 August 1988; pp. 41–50.
20. Hu, G.; Dam-Johansen, K.; Wedel, S.; Hansen, J.P. Decomposition and oxidation of pyrite. *Prog. Energy Combust. Sci.* **2006**, *32*, 295–314. [CrossRef]
21. Liu, Y.D.; Jia, M.; Xie, M.Z.; Pang, B. Development of a new skeletal chemical kinetic model of toluene reference fuel with application to gasoline surrogate fuels for computational fluid dynamics engine simulation. *Energy Fuels* **2013**, *27*, 4899–4909. [CrossRef]
22. Ranjan, S.; Sridhar, S.; Fruehan, R.J. Reaction of FeS with simulated slag and atmosphere. *Energy Fuels* **2010**, *24*, 5002–5007. [CrossRef]
23. Wu, S.; Huang, S.; Wu, Y.; Gao, J. Characteristics and catalytic actions of inorganic constituents from entrained-flow coal gasification slag. *J. Energy Inst.* **2015**, *88*, 93–103. [CrossRef]
24. Zhang, Z.; Wu, X.; Zhou, T.; Chen, Y.; Hou, N.; Piao, G. The effect of iron-bearing mineral melting behavior on ash deposition during coal combustion. *Proc. Combust. Inst.* **2011**, *33*, 2853–2861. [CrossRef]
25. Li, Q.H.; Zhang, Y.G.; Meng, A.H.; Li, L.; Li, G.X. Study on ash fusion temperature using original and simulated biomass ashes. *Fuel Process. Technol.* **2013**, *107*, 107–112. [CrossRef]
26. Li, C.-Z. *Advances in the Science of Victorian Brown Coal*; Elsevier: Amsterdam, The Netherlands, 2004.
27. Helble, J.J.; Srinivasachar, S.; Boni, A.A. Factors influencing the transformation of minerals during pulverized coal combustion. *Prog. Energy Combust. Sci.* **1990**, *16*, 267–279. [CrossRef]
28. Khadse, A.N. Resources and economic analyses of underground coal gasification in India. *Fuel* **2015**, *142*, 121–128. [CrossRef]
29. *ASTM Standard D3173-11. Test Method for Moisture in the Analysis Sample of Coal and Coke*; ASTM International: West Conshohocken, PA, USA, 2011.
30. *ASTM Standard D3175-11. Test Method for Volatile Matter in the Analysis Sample of Coal and Coke*; ASTM International: West Conshohocken, PA, USA, 2011.
31. *ASTM Standard D3174-11. Annual Book of ASTM Standards. Test Method for Ash in the Analysis Sample of Coal and Coke*; ASTM International: West Conshohocken, PA, USA, 2011.
32. *ASTM Standard D3177-02. Test Methods for Total Sulfur in the Analysis Sample of Coal and Coke*; Reapproved 2007; ASTM International: West Conshohocken, PA, USA, 2002.
33. Takagi, H.; Maruyama, K.; Yoshizawa, N.; Yamada, Y.; Sato, Y. XRD analysis of carbon stacking structure in coal during heat treatment. *Fuel* **2004**, *83*, 2427–2433. [CrossRef]
34. Zeng, X.; Zheng, S.; Zhou, H.; Fang, Q.; Lou, C. Char burnout characteristics of five coals below and above ash flow temperature: TG, SEM, and EDS analysis. *Appl. Therm. Eng.* **2016**, *103*, 1156–1163. [CrossRef]
35. Dyk, J.C.V.; Melzer, S.; Sobiecki, A. Mineral matter transformation during Sasol-Lurgi fixed bed dry bottom gasification—Utilization of HT-XRD and FactSage modelling. *Miner. Eng.* **2006**, *19*, 1126–1135.
36. Li, W.; Bai, J. *Chemistry of Ash from Coal*; Science Press: Beijing, China, 2013; p. 43. (In Chinese)

37. Wang, H.; Qiu, P.; Wu, S.; Yun, Z.; Li, Y.; Zhao, G. Melting behavior of typical ash particles in reducing atmosphere. *Energy Fuels* **2012**, *26*, 3527–3541. [CrossRef]
38. Ward, C.R. Analysis and significance of mineral matter in coal seams. *Int. J. Coal Geol.* **2002**, *50*, 135–168. [CrossRef]
39. Dai, S.; Ren, D.; Chou, C.L.; Finkelman, R.B.; Seredin, V.V.; Zhou, Y. Geochemistry of trace elements in Chinese coals: A review of abundances, genetic types, impacts on human health, and industrial utilization. *Int. J. Coal Geol.* **2012**, *94*, 3–21. [CrossRef]
40. Ward, C.R. Analysis, origin and significance of mineral matter in coal: An updated review. *Int. J. Coal Geol.* **2016**, *165*, 1–27. [CrossRef]
41. Dai, S.; Li, D.; Chou, C.L.; Zhao, L.; Zhang, Y.; Ren, D. Mineralogy and geochemistry of boehmite-rich coals: New insights from the Haerwusu surface mine, Jungar coalfield, Inner Mongolia, China. *Int. J. Coal Geol.* **2008**, *74*, 185–202. [CrossRef]
42. Dai, S.; Wang, X.; Seredin, V.V.; Hower, J.C.; Ward, C.R.; O'Keefe, J.M.K. Petrology, mineralogy, and geochemistry of the Ge-rich coal from the Wulantuga Ge ore deposit, Inner Mongolia, China: New data and genetic implications. *Int. J. Coal Geol.* **2012**, *90–91*, 72–99. [CrossRef]
43. Dai, S.; Liu, J.; Ward, C.R.; Hower, J.C.; Xie, P.; Jiang, Y. Petrological, geochemical, and mineralogical compositions of the low-Ge coals from the Shengli Coalfield, China: A comparative study with Ge-rich coals and a formation model for coal-hosted Ge ore deposit. *Ore Geol. Rev.* **2015**, *71*, 318–349. [CrossRef]
44. Wu, X.; Zhou, T.; Chen, Y.; Zhang, Z.; Piao, G.; Kobayashi, N. Mineral melting behavior of Chinese blended coal ash under gasification condition. *Asia Pac. J. Chem. Eng.* **2011**, *6*, 220–230. [CrossRef]
45. Ding, T. Tonsteins: Altered volcanic-ash layers in coal-bearing sequences: Bruce F. Bohor and don m. Triplehorn. Special paper no. 285, The Geological Society of America, 1993, 44p. US $24.00 (ISBN 0-8137-2285-3). *Geochim. Cosmochim. Acta* **1994**, *58*, 1–44.
46. Dai, S.; Ward, C.R.; Graham, I.T.; French, D.; Hower, J.C.; Zhao, L. Altered volcanic ashes in coal and coal-bearing sequences: A review of their nature and significance. *Earth Sci. Rev.* **2017**, *175*, 44–74. [CrossRef]
47. Liu, S.; Qi, C.; Jiang, Z.; Zhang, Y.; Niu, M.; Li, Y. Mineralogy and geochemistry of ash and slag from coal gasification in China: A review. *Int. Geol. Rev.* **2017**, 1–19. [CrossRef]
48. Żogała, A.; Janoszek, T. CFD simulations of influence of steam ingasification agent on parameters of UCG process. *J. Sustain. Min.* **2015**, *14*, 2–11. [CrossRef]
49. Dai, S.; Ren, D.; Zhou, Y.; Chou, C.L.; Wang, X.; Zhao, L. Mineralogy and geochemistry of a superhigh-organic-sulfur coal, Yanshan Coalfield, Yunnan, China: Evidence for a volcanic ash component and influence by submarine exhalation. *Chem. Geol.* **2008**, *255*, 182–194. [CrossRef]
50. Jin, B.; Li, W.; Bai, Z. Effects of mineral matter and coal blending on gasification. *Energy Fuels* **2011**, *25*, 1127–1131.
51. Matjie, R.H.; Li, Z.S.; Ward, C.R.; French, D. Chemical composition of glass and crystalline phases in coarse coal gasification ash. *Fuel* **2008**, *87*, 857–869. [CrossRef]
52. WU, X.J.; Zhang, Z.X.; Zhou, T.; Chen, Y.S.; Chen, G.Y.; Cheng, L.U. Ash fusion characteristics and mineral evolvement of blended ash under gasification condition. *J. Combust. Sci. Technol.* **2010**, *16*, 508–514.
53. Grim, R.E. *Clay Mineralogy*, 2nd ed.; McGraw-Hill Book Company: New York, NY, USA, 1968; p. 173.
54. Moustakas, K.; Mavropoulos, A.; Katsou, E.; Haralambous, K.J.; Loizidou, M. Leaching properties of slag generated by a gasification/vitrification unit: The role of pH, particle size, contact time and cooling method used. *J. Hazard. Mater.* **2012**, *207–208*, 44–50. [CrossRef] [PubMed]